Troitzsch, Constanze; Marten, Anne-Katrin; Westermann, Dirk

Troitzsch, Constanze; Marten, Anne-Katrin; Westermann, Dirk

Original published in:

IET generation, transmission and distribution. - London : IET. - 10 (2016), 16, p. 4231-4239.

Original published: 2016-12-08
ISSN (online): 1751-8695
ISSN (print): 1751-8687
DOI: 10.1049/iet-gtd.2015.0700
URL: https://doi.org/10.1049/iet-gtd.2015.0700
[*Visited:* 2017-10-12]

IET Generation, Transmission & Distribution

Research Article

IET Journals
The Institution of Engineering and Technology

Non-telecommunication based DC line fault detection methodology for meshed HVDC grids

ISSN 1751-8687
Received on 29th June 2015
Revised on 16th June 2016
Accepted on 24th July 2016
doi: 10.1049/iet-gtd.2015.0700
www.ietdl.org

Constanze Troitzsch[1], Anne-K. Marten[2] ✉, Dirk Westermann[2]

[1]*Swissgrid AG, Werkstrasse 12, 5080, Laufenburg, Switzerland*
[2]*Department of Power Systems, Technische Universität Ilmenau, Gustav-Kirchhoff-Str. 1 98693 Ilmenau, Germany*
✉ *E-mail: anne-katrin.marten@tu-ilmenau.de*

Abstract: One of the most challenging aspects regarding realisation of meshed high-voltage direct current (HVDC) systems is the handling of DC line faults. Due to the specific DC fault current phenomena, AC fault detection and clearance methods are not applicable in meshed HVDC grids. New fault clearing algorithms and equipment need to be developed. Therefore it is necessary to be aware of the DC fault current characteristics. Starting from a travelling wave approach simplifications for fault currents in low – and high impedance earthed DC grids are derived. On this basis, a non-telecommunication based DC fault detection algorithm is designed. Due to its decentralised implementation, it is very fast acting, reliable and economic in comparison with centralised approaches which are characterised by a parallel telecommunication system. Furthermore it is able to detect pole to pole as well as pole to earth faults in low- and high-impedance earthed DC grid. Finally this fault detection algorithm is validated by numerical case studies.

1 Introduction

Worldwide many efforts are being directed to provide engineering solutions for a meshed high-voltage direct current (HVDC) overlay grid. In the long run it is supposed to design a new network level in Europe in order to reliably transmit bulk power over long distances. As a meshed HVDC grid has to relieve the existing AC system, it must be highly available and redundant. Thus the implementation of an adequate network protection system is of great importance. Due to the lack of natural zero crossings and rapid rise of DC-side fault currents the use of existing AC protection techniques is not feasible in general. But nonetheless the development of a DC-side-protection system should be guided by the protection requirements that are well established in AC-systems. These are reliability, rapidity, economy, selectivity and accuracy. In order to design an HVDC protection scheme the occurring DC fault current characteristics must be known to derive criteria for fault detection. This paper intends to give a rough estimate about the possibility to create a protection system based on local measurements to be fast enough to deal with the DC fault currents. Thus worst case analyses are made provoking the need for very fast detection. The paper roughly describes characteristics of DC fault currents caused by DC line faults by means of travelling wave theory. Based on these gained DC fault current and voltage characteristics thresholds are defined as a fundament for a non-telecommunication based fault detection concept.

Nowadays, DC fault current calculation in HVDC systems is not standardised. In IEC 61660-1 a method for calculating short circuit currents in DC auxiliary systems is described [1]. This standard defines the DC fault current to be a superposition of several partial currents that are fed from converters, batteries, capacitances and DC motors. Since auxiliary systems are limited in space, IEC 61660-1 considers neither the impact of meshed links, nor transmission line parameters. That is why this standard cannot be applied to meshed expanded HVDC grids. Thus, other methods to describe DC fault currents have to be analysed. Several papers investigate DC fault currents in HVDC systems based on simulations but without deeper analysis, e.g. on a mathematical level or a description of the used methods as in [2–4].

The results obtained from DC fault current analysis form the basis for definition of criteria for DC fault detection. Existing approaches are based on the detection of wave fronts generated by DC fault using wavelet transformation [5–7]. Due to the complex propagation of fault current and voltage waves in meshed HVDC networks an universal fault detection method based on this principle is difficult to implement and has not been published yet. Other approaches suggest the use of current or rather voltage gradients as detection criteria whereupon the application in meshed DC grids is not discussed [8]. Furthermore, the differential current protection, which is also well established in three-phase AC systems, is proposed for fault detection in meshed HVDC grids [9]. This highly selective criterion is realised by comparing the current at the beginning and at the end of a transmission line, so that a parallel telecommunication link must be available. Thus, the feasibility of this approach is problematic in HVDC systems with transmission line lengths of several hundred kilometres especially with regard to an onshore overlay grid that might be built in the future [10]. In [9], the signal propagation time on a 200 km long fibre optic cable is assumed to be 1 ms. Since the rise of the fault currents is in the range of a few kA/ms, a delay of 1 ms per 200 km is not negligible. In addition, the reliability of the entire protection system would depend on telecommunication system's availability whose installation causes additional costs. Thus telecommunication based DC protection systems are not acceptable due to economic and reliability reasons. Hence, a local detection principle should be preferred. Some of the identified disadvantages are overcome by the handshaking method described in [11]. In this combined fault detection and clearing process all converters of a HVDC system are involved. This approach is not applicable in geographical wide expanded HVDC grids due to the lack of selectivity and rapidity.

The method proposed in this paper does not rely on a telecommunication system and thus overcomes the identified disadvantages of existing approaches. It takes up the idea of analysing arriving current and voltage wave fronts at each HVDC grid node and examines the possibility of selectively identifying the faulted DC line. The local analysing of three criteria ensures a reliable identification of fault type and fault location in meshed and radial HVDC topologies within a very short time depending on line length much faster than one millisecond.

Section 2 depicts the model used for fault current characteristic description in the same section. The starting point for fault current

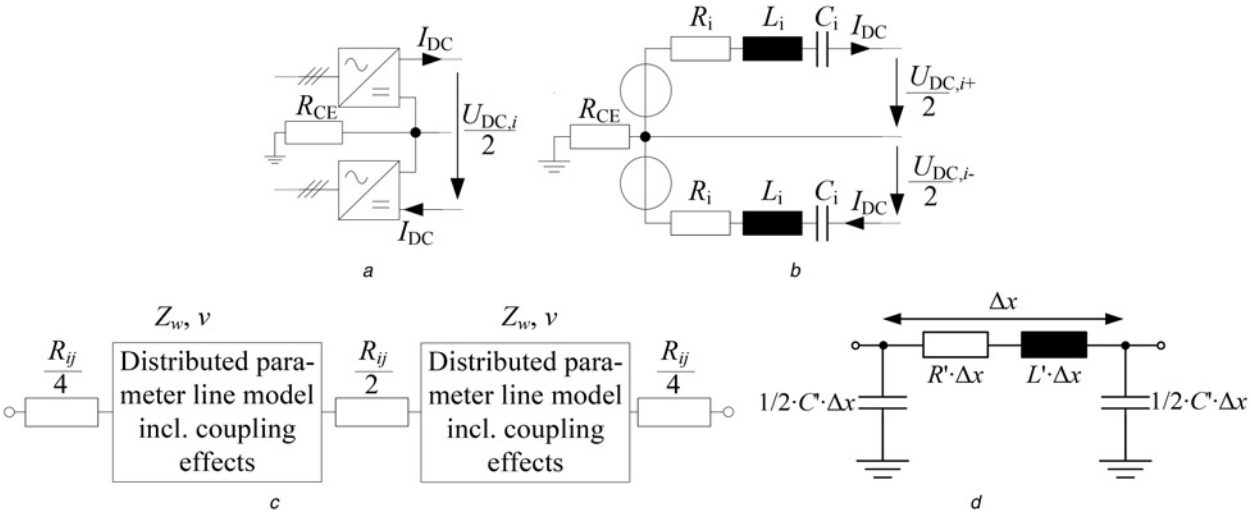

Fig. 1 *Converter and transmission line models*

a Converter model – simplified scheme
b Converter model – equivalent circuit diagram [14–17]
c Transmission line model – simplified scheme of a distributed parameter line model including lumped losses
d Transmission line model – π-line-segment

analysis is the travelling wave theory, which is the basis of a simplified description of a fault current calculation approach for low impedance earthed grids. Based on fault current characteristics a DC line fault detection algorithm is proposed in Section 3. An excerpt of numerical simulation results for verification of the proposed DC fault detection algorithm is given in Section 4. Finally a conclusion is depicted in Section 5.

2 Fault current characterisation

This section describes fault current characteristics within HVDC systems. Starting from a general approach outlining the propagation of fault currents in DC systems based on travelling wave theory, approximations of these fault currents in high- and low-impedance earthed HVDC-grids are derived. To obtain the general shape of the fault current's curves, theoretical worst case scenarios are considered neglecting on the one hand asset's parameters and on the other converter's inner protection, which would limit the fault current after a few milliseconds in real implemented systems. Therefore, the main focus is concentrated on the time span right after fault inception as a base for a reliable fault detection algorithm.

2.1 Model

The implementation of meshed HVDC grids is solely feasible with voltage source converters, thus modular multi-level converters (MMC) are taken as a basis [12, 13]. Their equivalent circuit diagram in normal operation can be assumed as a voltage source with an internal series resistance R_i, inductance L_i and capacitance C_i (Fig. 1*b*). L_i and C_i must only be considered in transient analyses. U_{DC} and I_{DC} represent the converter's DC side output voltage and output current. In addition, R_{CE} comprises the resistance between earth and the electrical midpoint of the two serial converters of a converter bipole. Since the main scope of this paper is the fault current in the beginning (right after fault inception), voltage source's output is assumed not to change. Hence the modelling of MMC's sub-modules and furthermore converter's inner protection is not taken into account. This assumption is permissible as it is intended to design a fault detection algorithm acting very fast in order to have enough time for fault interruption. In real installations, this model is only valid until the beginning of the internal converter (overcurrent) protection of full bridge converters which normally reduces the DC voltage in disturbed situations in order not to exceed $1.3*I_{nominal}$.

According to the bipolar converter model transmission lines are considered to be bipolar as well (see Fig. 1*a*), since more power can be transmitted by the use of the same insulation level and a certain level of redundancy can be provided using this topology depending on neutral conductors level of insulation and converter switchyard topology [18]. Furthermore, a neutral conductor is carried in parallel which is out of service in normal operations. This can be used in case of a tripped pole/line to transmit at least the half of the power (medium voltage insulation level) or full power (nominal DC voltage insulation level of neutral conductor) [18]. Depending on the scope of the analyses different transmission line models are used [19]. To describe travelling wave phenomena a distributed parameter line model based on the Bergeron travelling wave method which also takes into account coupling effects between the conductors and losses is used. For simulations Matlab/Simulink's SimPowerSystems toolbox is used. In this approach each single phase line is basically characterised by a surge impedance Z_w and a propagation velocity v as described in (1) and (2), where L' is the specific inductance and C' the specific capacitance of a transmission line. Losses are taken into consideration by SimPowerSystems toolbox as lumped losses by distributing $R/4$ at each end of a lossless line and $R/2$ in the middle of the line (see Fig. 2*c*).

$$Z_w = \sqrt{\frac{L'}{C'}} \tag{1}$$

$$v = \frac{1}{\sqrt{L' \cdot C'}} \tag{2}$$

Moreover, analyses that aim to achieve approximations are based on several serial π-line-models. In this approach a single segment of the length Δx is depicted in Fig. 1*c*, where R' is the specific resistance, L' the specific inductance and C' the specific capacitance. The specific conductance G' is neglected in this approach.

2.2 DC fault characteristics

Faults affecting HVDC systems can either be located on the AC-side, inside the converter, in the DC switch yard or on the DC transmission lines. This paper focuses on the latter case and on transversal faults. In the first part of this section, the travelling

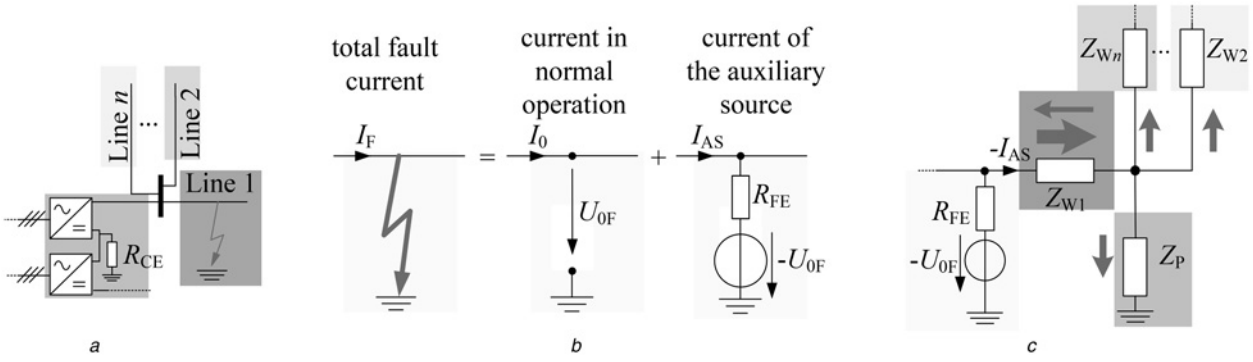

Fig. 2 *Fault location modelling and propagation of fault current and voltage waves*

a Simplified scheme of a converter's node connected to a faulty line
b Fault current composition at the fault location
c Equivalent circuit diagram of a converter's node including the principle of fault current wave's propagation

wave characteristic of DC-fault current is derived. Based on this, approximation for fault currents in high and low resistance networks are deduced.

2.2.1 Travelling wave characteristics: Irrespective of the fault type the total DC side fault current I_F can be assumed to be a superposition of the pre-fault line current I_0 and a fault current component I_{AS} fed by an auxiliary source. This approach is comparable with the Thevenin-theorem established in the fault current's calculation in multi-infeed three phase AC networks. In transversal fault scenarios, the auxiliary source is a voltage source either between both poles (for pole to pole-faults) or between one pole and ground (for pole to earth-faults). In the latter case which is illustrated in Fig. 2*b* and derived from Fig. 2*a*, the value of the auxiliary sources changes between zero and the negative value of the pre-fault voltage at fault location U_{F0}. In addition, R_{FE} represents the fault and earth resistance at the fault location. The shape of the auxiliary source is determined by the fault occurrence conditions, which can be a step function in a theoretical worst case.

In accordance with the same methodology, the fault current for longitudinal faults can be calculated by replacing the transversal voltage source by a series current source within the line. During fault inception its amplitude changes between zero and the negative value of the pre-fault line current I_0.

After fault inception a voltage is impressed at the fault location, which propagates in form of a wave towards both converter nodes of a line. This wave is refracted and reflected at discontinuities in the grid (e.g. converter node) and interferes as a result to the particular fault current I_{AS} (see Fig. 2*c*). A measure of the fault waves' propagation in the grid can be estimated by the refraction coefficient b at the converter's node calculated generally as follows

$$b = 1 + \frac{(Z_{w,eq} - Z_{w1})}{(Z_{w,eq} + Z_{w1})} \tag{3}$$

$$Z_{w,eq} = \frac{1}{\left((1/Z_{w2}) + \ldots + (1/Z_{wn}) + (1/Z_P)\right)} \tag{4}$$

Z_{w1} is the surge impedance of the faulty line which includes as well the serial part of the converter's inner inductance and $Z_{w,eq}$ an equivalent surge impedance of the branches directly connected to the converter's node. $Z_{w,eq}$ includes the surge impedances of the direct adjacent $(n-1)$ lines Z_{w2}, …, Z_{wn} and Z_P which represents the parallel component of the converter's surge impedance as well as the ground resistance R_{CE}.

Hence, it follows that the propagation of fault waves depends on the relation of the surge impedances. In low impedance earthed grids the ratio Z_P to Z_{w1}, Z_{w2},…, Z_{wn} is much smaller than in high impedance earthed grids. Thus the refraction factor b is smaller in low impedance than in high impedance earthed grids, which means that the part of the entire fault current that stays in the faulty branch is higher than the other leaving it. In high impedance earthed grids, Z_P is in the range of the surge impedances or even much higher. Thus, the refraction factor b in these grids is always significantly higher than in low impedance earthed grids so that a larger part of the fault current and voltage waves propagate into the adjacent grid.

Consequently, a distinction must be made between short circuit currents for low-impedance and earth leakage currents for high-impedance earthed (Fig. 1*b*) grids.

2.2.2 Approximation in low impedance earthed grids – short circuit currents: If the converter's earthing resistance R_{CE} is close to zero, the fault current path is closed over earth, which is illustrated in Fig. 3*a* for a positive pole to earth fault on a simple point-to-point (P2P) connection. In order to consider a worst-case scenario, the converter's inner inductance is not considered in the following section since it would limit the slope of the fault current contribution of the converter. To deduce a simplified equation of the fault current, the equivalent circuit in Fig. 3*b* is derived with the help of the π-line model. In this case, the converter voltage drops over the converter's inner resistance R_{i1} and R_{i2}, the earth and fault impedance R_{FE} as well as over the lumped resistive and inductive line parameters R_{1F}, R_{2F}, L_{1F} and L_{2F}. Since transmission lines are optimised with regard to minimal losses, their specific resistance and inductance are small and hence high fault currents with strong increases are the consequence.

On the basis of the simplified equivalent circuit in Fig. 3*b* and the reduced loop analysis [20] the two fault currents I_{F1} and I_{F2} can be defined in a simplified way as in (5). The matrix $\boldsymbol{Z}$ and the vector $\boldsymbol{w}$ are defined as in (6) and (7). The elements correspond to concentrated elements in Fig. 3*b* and converter representation as previously described in Fig. 1 for the disturbed pole. The current I_0 represents the line current just before the fault occurrence as described in Fig. 3*c*. Furthermore, s represents the variable in the Laplace domain.

$$\begin{pmatrix} I_{F1}(t) \\ I_{F2}(t) \end{pmatrix} = \begin{pmatrix} 1 \\ -1 \end{pmatrix} \cdot \mathcal{L}^{-1}\{\boldsymbol{Z}^{-1} \cdot \boldsymbol{w}\} \tag{5}$$

$$\boldsymbol{Z} = \begin{pmatrix} R_{i1} + R_{1F} + R_{FE} + s \cdot L_{1F} & -R_{FE} \\ -R_{FE} & R_{i2} + R_{2F} + R_{FE} + s \cdot L_{2F} \end{pmatrix} \tag{6}$$

$$\boldsymbol{w} = \begin{pmatrix} \dfrac{U_{DC1}}{s} + L_{1F} \cdot I_0 \\ -\dfrac{U_{DC2}}{s} + L_{2F} \cdot I_0 \end{pmatrix} \tag{7}$$

Fig. 3*c* shows the fault current results from the travelling wave simulation using SimPowerSystem toolbox (taking into account transverse parameters, distributed parameters, modal

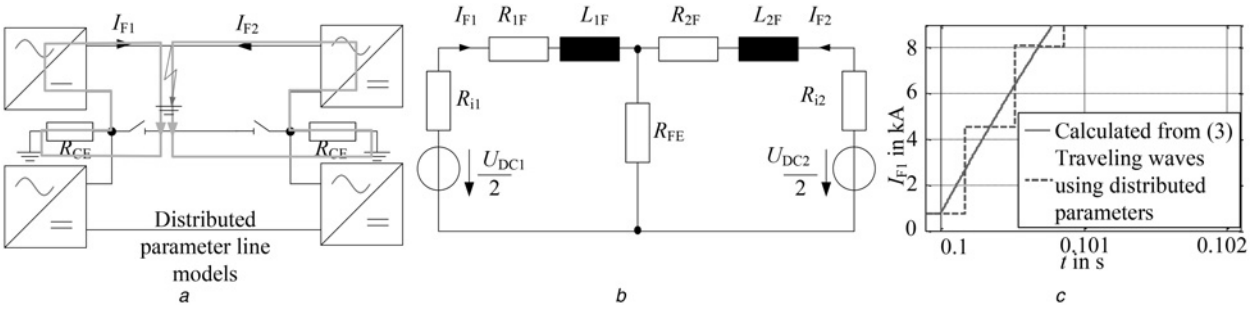

Fig. 3 *Pole to earth short circuit on the positive (disturbed) pole of a P2P connection*

a Simplified scheme
b Equivalent circuit diagram for derivation of the approximately formula in a low impedance earthed system
c Graph of the pole to earth short-circuit current

transformation for the multi conductor system and travelling waves) and those from the simplified model in Fig. 3*b* as described in (5). The results are obtained for the fault current I_{F1} fed by converter 1 and 2. The parameters for the investigated HVDC grid topology are shown in Table 1.

The step function shape of the dashed curve representing travelling wave simulation is the result of the simulation considering the worst case scenario of an abrupt fault occurrence. Further, the calculated graph that is drawn through using (5) approximates the simulated graph very well. If the short circuit current would not be limited by the converter's inner protection, it would theoretically reach a dimension of hundredfold of the current compared with normal operation depending on the system parameters and neglecting the equipment's limits. According to (5)–(7), major influencing quantities that affect the maximum amplitude of the short circuit current are voltage level, specific line resistance, fault position on the line, earth resistance and fault impedance. In addition, the slope of this fault current is mainly influenced by the specific line inductance and voltage level and reaches dimensions right up to 10 kA/ms ($U_n = 800$ kV) and 6-7 kA/ms ($U_n = 500$ kV) whereby inductances of typical HVDC overhead transmission lines are considered (as in Table 1). If the specific inductance would be even smaller (e.g. $L' = 0.5$ mH/km in the case of HVDC cable transmission lines), fault current slope for 500 kV systems would increase to 10 kA/ms as well.

2.2.3 Approximation in high-impedance earthed grids – earth leakage currents: In high impedance earthed grids in which the resistance R_{CE} (Fig. 1*b*) is very high compared with the surge impedances of the lines, the fault current path is closed over the distributed line and the converter's inner capacitance. Since the fault current waves propagate in the adjacent branches, the final fault current is fed by the distributed capacitances of the entire grid. An example scenario is shown in Fig. 4*a* for the illustrated P2P connection based on two concentrated capacitances. Due to the non-linear interaction of all line capacitances, it is not feasible to deduce a closed equation with the aid of the linear network theory.

An qualitative approximation of the real fault current is achievable by partitioning the line in several series connected π-equivalents, where the initial voltage over all capacitances in the grid is the pre-fault pole to earth voltage at the fault location U_{F0} (Fig. 2*b*). The shape of the resulting earth leakage current depends on the DC line's specific capacitance, since the feeding capacitances form a series resonant circuit with the line inductances. In networks including small capacitances (e.g. grids based on overhead transmission lines) the earth leakage current curve is sinusoidal. The larger the capacitances in a grid are (e.g. in extended cable networks), the more the fault current will appear with an aperiodic shape. The fault current I_{F1} that would result in both cases for the discussed P2P-connection is illustrated in Figs. 4*b* and *c*.

The two results obtained from this investigation are compared with the curves generated by a distributed parameter line model. It is shown, that the approximation approaches the fault current obtained from the simulation of a distributed parameter line model very well whose shape results again from the abrupt fault entering. Furthermore, the more π-equivalents are implemented the better the approximation becomes.

In contrast to short circuit currents, the terminal value of the earth leakage current I_{AS} is always zero due to the discharge of the capacitances. The maximum value of this fault current depends primarily on the specific capacitance of the transmission lines, the voltage level and the grid expansion. The magnitude of the first half-wave reaches the dimension right up to decuple of the current in normal operation for an overhead transmission line system. In cable systems it is much larger. Nonetheless the earth leakage current is smaller than the short circuit current, but the approximately doubling of the voltage on the healthy pole must be taken into account when developing a high resistance earthed system. Furthermore, the specific inductance of a line and the voltage level primarily affect fault current rise during fault occurrence. The gradient reaches values up to 10 kA/ms for grids with nominal voltage of $U_n = 800$ kV and 6–7 kA/ms for grids with nominal voltage of $U_n = 500$ kV as in the case of a short circuit.

Table 1 Parameters of considered P2P connection

Description	Parameter	Value
voltage at node 1	U_{DC1}	500 kV
voltage at node 2	U_{DC2}	495 kV
specific line resistance	R'	0.01 Ω/km
specific line inductance	L'	0.863 mH/km
specific line capacitance	C'	13.8 nF/km
total line length	l_T	200 km
fault distance to node 1	l_{1F}	50 km
fault and earth resistance	R_{FE}	6 Ω
inner converter resistance	$R_i = R_{i1} = R_{i2}$	0.5 Ω

3 Non-telecommunication based DC line fault detection methodology

The implementation of a fault detection methodology must be based on the knowledge of the characteristics of the occurring fault currents. The design of an HVDC fault detection concept should be orientated on the requirements established and proved in existing three phase AC systems. Thus a DC protection system must be very fast because of the high rises of the DC fault currents (see Section 2). Further, it must be selective and sensitive to avoid false detection and unnecessary protection trips. Beside this, a DC fault detection concept should be realised without telecommunication to be economically, reliable and fast enough in HVDC grids with huge geographic extensions with line length of some hundred kilometres. In a first step, a converter and DC-substation protection should be implemented, which is not the scope of this paper. Afterwards, a DC line fault detection concept should be applied which evaluates several criteria (ΔI, ΔU and I_E) at each branch off point in the HVDC grid (decentralised

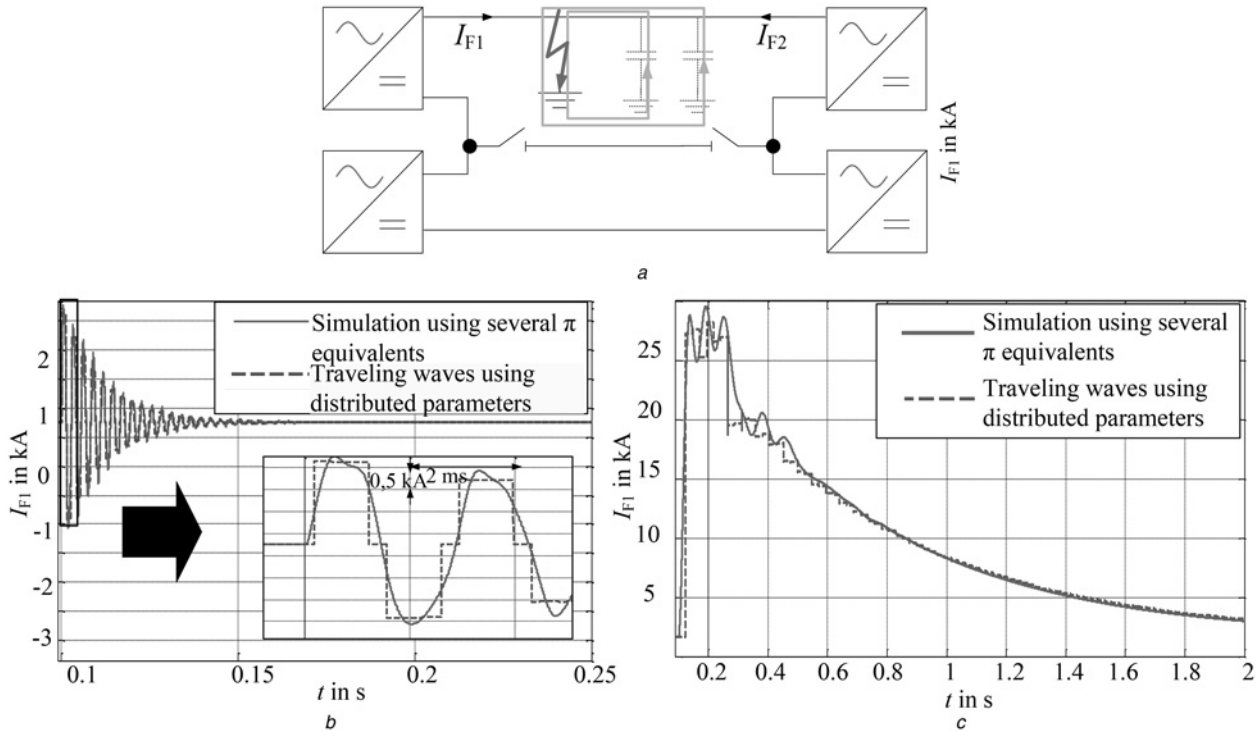

Fig. 4 *Pole to earth short circuit on the positive (disturbed) pole of a P2P connection*

a Simplified scheme including distributed capacitances
b Sinusoidal fault current on an overhead transmission line with a specific capacitance of 13.8 nF
c Aperiodic fault current on a cable transmission cableline with a specific capacitance of 255 μF

detection). Finally, to avoid a malfunction of the detection concept, a back-up protection is designed.

3.1 Step 1: Differential current protection for DC switch yard

In the first step, based on the differential current criterion, it is checked whether a fault is located on the line between the converter and DC switch yard or in the DC switch yard itself. If a fault has been detected in this manner, substation protection is triggered and the DC line protection system is disabled to avoid false tripping on non-faulty DC lines. Otherwise the algorithm proceeds to step 2.

3.2 Step 2: Evaluation of ΔI-, ΔU- and I_E-criterion

This evaluation step is the main part of the proposed protection algorithm. It continuously evaluates in parallel:

- the line current in each outgoing branch (ΔI-criterion)
- the pole to earth voltage (ΔU-criterion) and
- the current in the path of R_{CE} in Fig. 1*b* (ΔI_E-criterion) at converter's node.

All three methods are independent of each other. The basic procedure for detecting faults on a DC transmission line that is directly connected to a converter with the help of the ΔI-, ΔU- and I_E-criterion is illustrated in Fig. 5*a*. This ensures a high selective fault detection. In the first step (2a) it is checked whether there is any line fault in the DC grid. If this is true, the analysis continues to identify the fault type (step 2b). Finally the faulty branch is identified in step 2 c.

The ΔI-criterion analyses gradients of DC line currents on the positive and negative pole of each transmission line. In order to avoid false tripping, e.g. due to signal noise, not the current slope di/dt, but rather the change in current ΔI within a predefined time interval Δt is measured. In a first step, ΔI is compared with an a priori defined threshold ΔI_{trig} (step 2a). The values of the parameters ΔI_{trig} and Δt must be adjusted to first fault current waves that can arrive at a node at which the protection system is installed. Basically they depend on the grid meshing, the transmission line's length and parameters as well as on the system's earthing. In order to avoid an overestimation of the protection system ΔI_{trig} must be high enough not to initiate immediately the clearing process in case of a fault in an adjacent node or because of a change of the operation point. In the same context, the sampling time Δt must be high enough to avoid false detection due to signal noise. Furthermore, to prevent underestimation of the protection system, ΔI_{trig} should also cover the comparatively small fault current waves when the system is operated at its lower voltage range. Thus, ΔI_{trig} is defined according to (8) assuming the worst case (minimum allowed DC voltage). Consequently, if ΔI exceeds ΔI_{trig} within the predefined time interval Δt a DC line fault is detected. If the allowed voltage level is defined to be ±5% of the nominal DC voltage U_{DCn}, (9) shows the difference between the maximum possible change in DC line current as a consequence of an operating point change ΔI_{max} compared with the fault current trigger level ΔI_{trig}. In a second step the gradients on the positive (ΔI_p) and negative (ΔI_n) pole must be compared with each other (step 2b).

$$\Delta I_{trig} = 0.9 \cdot \frac{U_{DC,min}}{Z_w} \tag{8}$$

$$\begin{aligned}\Delta I_{trig} = 0.9 \cdot \frac{U_{DC,min}}{Z_w} = 0.9 \cdot \frac{0.95 \cdot U_{DCn}}{Z_w} = 0.855 \cdot \frac{U_{DCn}}{Z_w} > \\ > 0.1 \cdot \frac{U_{DCn}}{Z_w} = \frac{U_{DCmax} - U_{DCmin}}{Z_w} = \frac{(1.05 - 0.95) \cdot U_n}{Z_w} \\ = \Delta I_{max}\end{aligned} \tag{9}$$

If ΔI_p and ΔI_n are equal in magnitude by considering a certain degree of uncertainty but differ in sign, a pole to pole fault is located on the related line. Otherwise, if one of these gradients is greater than a

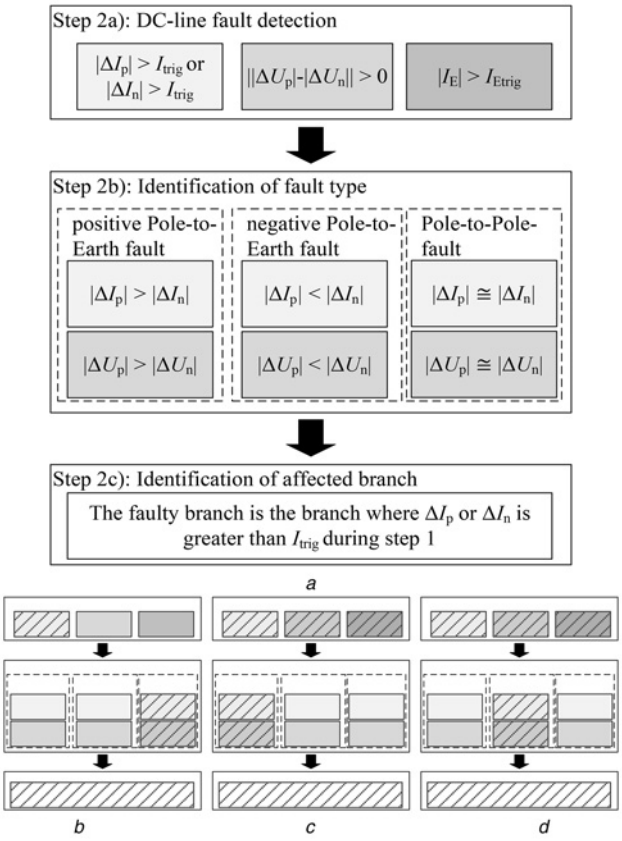

Fig. 5 *Basic procedure of combining the ΔI-, ΔU- and I_E-criterion at converter's node directly linked to a faulty branch. For sake of simplicity, factors for handling uncertainties during the measurement in real installations are not illustrated. The depiction of figures b, c and d are based on figure a. In these, the expected detection results for each fault type are highlighted the help of a striped rectangle*

a Basic protection procedure combining the ΔI-, ΔU- and I_E-criterion
b Expected results: pole to earth fault
c Expected results: positive pole to earth fault
d Expected results: negative pole to earth fault

predefined factor and also greater than the other at the same time, a pole to earth fault is situated on the pole that reaches the higher absolute value.

However, in case of a positive pole to earth fault the sign of ΔI_p is always negative since a negative voltage wave is impressed at the fault location (Fig. 2*b*) which causes in conjunction with the surge impedance a negative current wave. Vice versa, ΔI_n has a positive sign in a negative pole to earth scenario.

The ΔI criterion can precisely identify the fault type and fault location as indicated in Table 2.

In a high resistance earthed system, it is possible that ΔI_p and ΔI_n are equal in magnitude as well as in sign. In this case, the fault is not located on one of the outgoing lines but on a more remote link from the fault position since the fault current waves propagate in the entire grid.

The ΔI-criterion is able to detect pole to pole and pole to earth faults highly selective (identifies faulted line). Since in high resistance earthed systems more remote faults are detectable, a

Table 2 Detection criteria results for tripping when independently considering each criterion ((✓) – necessary criterion for fault detection, ✓ – sufficient criterion for line selectivity)

	Pole to pole short circuit	Pole to earth short circuit	Pole to earth leakage
ΔI-criterion	✓	✓	✓
ΔU-criterion	–	(✓)	(✓)
I_E-criterion	–	(✓)	(✓)

Table 3 Transmission line data

	Overhead line	Cable
R', Ω/km	0.010	0.010
L', mH/km	0.863	0.653
C' [OHL: nF/km, Cable: μF]	13.8	255.9

back-up protection based on the ΔI-criterion is conceivable as well. This is the main criterion of the proposed DC fault detection algorithm since it is highly selective.

The ΔU-criterion evaluates the gradients of pole to earth voltage at the positive (ΔU_p) and the negative pole (ΔU_n). This criterion is only pole but not line selective for transversal fault scenarios, since the pole to earth voltage is the same for all outgoing lines of one pole at the converter node. Thus this criterion is a necessary but not sufficient criterion for pole to earth faults as it is indicated in Table 2. A faulty state is detected based on step 2a) in Fig. 5*a*, if the absolute voltage value of one of the two pole voltages ΔU_p and ΔU_n related to a line changes more than the other. With reference to the step 2b) in Fig. 5*a*, the fault is situated on the pole with the higher voltage gradient.

In high resistance earthed networks it may happen that ΔU_p and ΔU_n are equal in magnitude as well as in sign. In this case, the fault is located on a remote link from the fault position. While this detection criterion is very fast, solely pole to earth faults are detectable.

In addition, the I_E-criterion evaluates the current in the branch of R_{CE} (Fig. 1*b*), which exists only in the case of a pole to earth fault. Thus, it is only possible to detect pole to earth fault scenarios (step 2a) in Fig. 5*a*) but without a deeper characterisation of the fault type and location as well as of the faulty branch (see Table 2). A pole to earth fault is detected if the absolute value of I_E is bigger than a predefined threshold I_{Etrig}, which is introduced to avoid false detection, e.g. because of signal noise or other disturbances.

The expected results of all three criteria in dependency of the fault type are summarised in Fig. 5*b–d*. The position of each field refers to Fig. 5*a*. The detection rules in all fault type scenarios are independent of the system's earthing.

If the evaluation of all parallel processed criteria achieves the results in Fig. 5*a*, the faulty branch is isolated from the grid in the following fault clearing process which is out of scope in this paper.

The earlier a fault wave reaches a node the earlier a protection device will be triggered. Hence, the detection methodology cannot be faster than the fault waves. An asynchronously fault clearing process on both sides of a line can result in case of a fault not located in the middle of the line. In consequence, once one side of the line is already switched off, the fault current commutates to the other side and if fault detection and clearing takes too long the remote protection equipment would have to switch off a much higher fault current. It is shown in Section 4 that this commutation process starts earliest once the fault clearance process is already

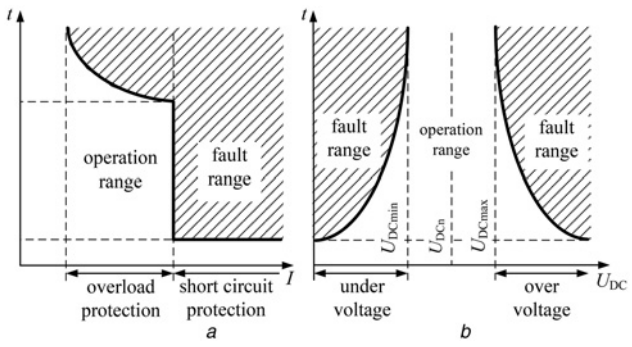

Fig. 6 *Backup protection*

a Delay current
b Delay voltage tripping curve

IET Gener. Transm. Distrib., 2016, Vol. 10, Iss. 16, pp. 4231–4239

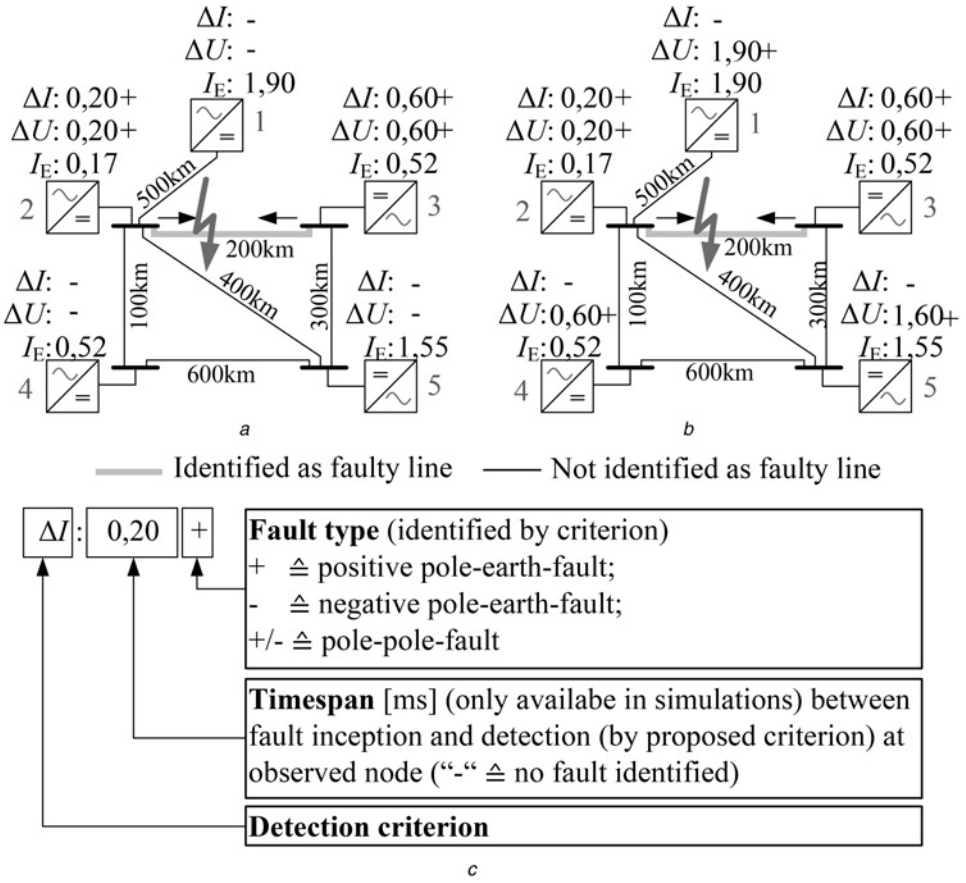

Fig. 7 *Detection results – overhead transmission lines*

a Short-circuit
b Earth-leakage
c Legend for the detection results in Figs. 7*a*, *b*, Figs. 8*a–c*

activated (fault has already been identified). Thus, an unsynchronised detection will not have a significant negative effect.

Furthermore to avoid false interpretation of the arriving travelling waves by the protection system due to travelling waves propagating in non-faulty branches of a node, it is proposed to install the measurement units of each branch in an appropriate distance to the busbar. This distance should be at least $v{\cdot}f^{-1}$ to the busbar, where v is the propagation velocity of the branch and f the sample rate of the measurement. If f is 1 MHz, this minimum distance should be for overhead line systems at least 0.3 mm and for cable systems 1.6 µm based on the values given in Table 3 (always fulfilled in substations). Furthermore, it is necessary to connect the devices of all branches of a node among each other. If a fault wave is detected by a device in the faulty branch, it would take at least $2/f$ until it reaches a device of a non-faulty branch. Depending on the protection concept, it is conceivable that the protection system blocks in this time the devices in the non-faulty branches to avoid unnecessary tripping.

Nonetheless, in case of a malfunction of the detection system in step 2a, 2b or 2c, e.g. due to defect measurement units, it may happen that a fault remains undiscovered. Then the algorithm proceeds to a backup-protection scheme in step 3.

3.3 Step 3: Backup protection – evaluating the operation ranges of line currents and pole to earth voltages

Since the fault state is characterised by currents and voltages leaving the operation range, it is possible to implement a back-up protection by checking the operational ranges of these variables with the aid of delay tripping curves. A possible characteristic for the DC line current is shown in Fig. 6*a*, which also includes an overload protection.

A similar curve of the pole to earth voltage is illustrated in Fig. 6*b*. With U_{DCmin} as the lower limit of the voltage operation range and U_{DCmax} as the upper limit, it is assured that the bigger the deviation of the operating range is, the faster the protection system will react.

4 Numerical simulations

Since step 2 is the central part of the fault detection algorithm, the functionality of the ΔI-, ΔU- and I_{E}-criterion is exemplarily tested for a pole to earth short circuit and a pole to earth leakage on a line within a meshed five node overhead transmission line 500 kV HVDC grid. All simulations are performed according to Section 2.1. The corresponding transmission system data are summarised in Table 3.

The fault location is defined to be 50 km apart from one converter and 150 km from the other to provoke unsynchronised fault detection on both line ends. The detection results of all three criteria at each node are summarised in Fig. 7*a* for a short circuit and Fig. 7*b* for an earth leakage. The corresponding legend is illustrated in Fig. 7*c*.

It is shown that the fault has been detected and correctly identified between node 2 and 3 according to Fig. 5*a* in both systems. Furthermore, the detection timespan is in both systems for all converters the same since the propagation velocity of the fault current and voltage waves solely depend on transmission line parameters. The fault is recognised earlier on node 2 than on node 3, because the fault location is closer to node 2. The only difference between both systems is that the faulty pole has been detected by all converters located far away from the faulty branch since the pole to earth voltage changes in case of a fault in a high

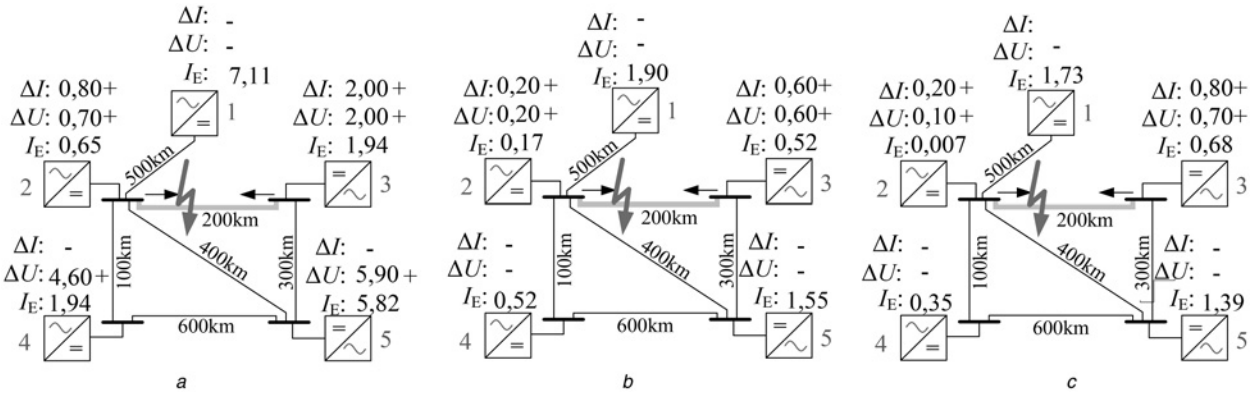

Fig. 8 *Detection results in a low impedance earthed HVDC grid (short circuits)*

a Cable transmission lines
b Low system voltage
c Fault location is close to converter 2

resistance earthing in the entire HVDC grid. Due to this similar fault detection behaviour in high and low impedance earthed HVDC grid, further investigations focus on short-circuit currents in low impedance earthed systems.

A major influencing factor on the described DC fault detection method is the transmission line technology. As cables have a higher specific capacitance as overhead transmission lines, the propagation speed on these is lower ((2)). Fault waves arrive later, hence the timespan according to Fig. 7*c* increases. This can be seen in Fig. 8*a*, where the detection results for a HVDC system solely consists of cables.

Another important point to consider is the fault detection in case of low system voltage which provokes the smallest initial fault currents and voltage waves that could occur. To avoid a malfunction, the protection system's parameters must be designed accurate to ensure a proper fault detection. Detection results for such a situation are summarised in Fig. 8*b*. It is assumed that the lowest voltage in the grid is equal to the lower voltage limit U_{DCmin} which is defined as $0.95{*}U_{\mathrm{DCn}}$ [21]. Thus, the average voltage in the grid is slightly higher than this. The obtained results mainly coincide with those in Fig. 7*a*. In summary, a low system voltage level has no significant impact on the fault detection system proposed in this paper.

Faults located close to the converter cause high currents with large slopes. Thus it must be ensured that they do not lead to false detection on adjacent non-faulty lines. The detection results of a fault in a distance $l_{2\mathrm{F}}$ of 2 km from the node 2 and $l_{3\mathrm{F}}$ of 198 km from node 3 are summarised in Fig. 8*c*. It can be seen that the fault is detected solely on the faulty line. Since the converter installed at node 2 recognises the fault in any case prior to the converter installed at node 3. Nonetheless, a commutation of the current from converter 2 to converter 3 during the fault clearing process is avoided due to the high speed of the presented detection principle, which is in the range of a fractional of a millisecond after fault waves arriving at the measuring point at the nodes. Thus, it can be assumed that the fault is simultaneously detected with the arriving fault wave fronts. According to Fig. 3*b*, the fault is detected at the closer located converter node after a time of $l_{2\mathrm{F}}/v$ and at the remote converter after a time of $l_{3\mathrm{F}}/v$. Thus, the entire current flowing through the converter 2 would commutate after a time of $l_{2\mathrm{F}}/v + t_{\mathrm{FC}} + (l_{2\mathrm{F}} + l_{3\mathrm{F}})/v$ at the converter 3, where t_{FC} is the fault clearing time at node 2 that depends on the type of the fault clearing process, respectively, equipment. Even if t_{FC} is zero, the time until the whole current through converter 2 is commutated to converter 3, is in any case higher than the time converter 3's fault detection needs to recognise the DC line fault. Since in practice t_{FC} is always greater than zero, the commutation process starts earliest when the fault clearance process is already activated at node 3. In conclusion in the case of a fault located close to a converter the fault clearance process at the corresponding node has no negative impact on the more remote converter.

5 Conclusions

For some years the possibility to build meshed HVDC grid is proposed to overcome challenges caused by increasing bulk power long distance transmission demand. Since AC systems and even today's P2P HVDC schemes have a different fault behaviour than a meshed HVDC grid there is an urgent research demand on fault detection and clearing within meshed HVDC grids. This paper proposes a non-telecommunication based DC fault detection methodology for meshed HVDC grids. The outlined method significantly improves state of the art algorithms.

A brief introduction into the state of the art of DC fault current calculation and DC fault detection methods is given. Existing standards for DC fault current calculation cannot be applied to geographically expanded and meshed HVDC grids. In this paper an HVDC grid fault detection scheme is proposed, that is selective, fast and independent of any telecommunication system.

DC fault current characteristics within meshed HVDC systems are identified for low and high impedance earthed systems. For low impedance earthed systems mathematical equations for simplified dynamic fault current calculation are defined. These results meet the results achieved with travelling wave simulations very well. For high impedance earthed systems a distributed parameter model is compared with a travelling wave simulation as well. For both system types current gradients just after the fault inception are in the range of 6–7 kA/ms for a 500 kV HVDC system.

The proposed detection algorithm is a distributed one and thus implemented at all DC nodes separately for each outgoing line (ΔI criterion). It continuously monitors branch currents, pole to earth DC node voltages for each pole and converter's neutral current. These measurements are evaluated by three criteria in parallel.

Several analyses are made in order to validate the proposed method. The functionality of the presented fault detection concept is independent of the transmission line technology, the system voltage level, the fault position on the line and detects all type of line faults selectively. Furthermore, operating point changes do not lead to a false detection.

6 References

1 Schlabbach, J.: 'Short-circuit currents' (The Institution of Electrical Engineering and Technology, 2005, 1st edn.)
2 Tang, L., Ooi, B.-T.: 'Locating and isolating DC faults in multi-terminal DC system', *IEEE Trans. Power Deliv.*, 2007, **22**, (3), pp. 1877–1884
3 Rafferty, J., Xu, L., Morrow, D.J.: 'DC fault analysis of VSC based multi-terminal HVDC systems'. Proc. IET Int. Conf. on AC and DC Power Transmission, Birmingham, United Kingdom, 2012, pp. 1–6
4 Tang, L., Ooi, B.-T.: 'Protection of VSC-multi-terminal HVDC against DC faults'. Proc. Annual Power Electronics Specialists Conf., Queensland, Australia, 2002, pp. 719–724
5 De Kerf, K., Srivastava, K., Reza, M., *et al.*: 'Wavelet-based protection strategy for DC faults in multi-terminal VSC HVDC systems', *IET Gener. Transm. Distrib.*, 2011, **5**, (4), pp. 496–503

6 Borghetti, A., Bosetti, M., Di Silvestro, M., *et al.*: 'Continuous-wavelet transform for fault location in distribution power networks: definition of mother wavelets inferred from fault originated transients', *IEEE Trans. Power Syst.*, 2008, **23**, (2), pp. 380–388
7 Magnago, F.H., Abur, A.: 'Fault location using Wavelets', *IEEE Trans. Power Deliv.*, 1998, **13**, (4), pp. 1475–1480
8 Naidoo, D., Ijumba, N.M.: 'HVDC line protection for the proposed future HVDC systems'. Proc. Int. Conf. on Power System Technology, Singapore, China, 2014, pp. 1327–1332
9 Descloux, J., Rault, P., Nguefeu, S., *et al.*: 'HVDC meshed grid: control and protection of a multi-terminal HVDC system'. CIGRÉ Session, Paper B4-308, Paris, 2012
10 Jovcic, D., van Hertem, D., Linden, K., *et al.*: 'Feasibility of DC transmission networks'. IEEE PES Int. Conf. and Exhibition on Innovative Smart Grid Technologies, Detroit, USA, 2011, pp. 1–8
11 Tang, L.: 'Control and protection of multi-terminal DC transmission systems based on voltage-source converters'. Dissertation, McGill University, 2003
12 Ahmed, N., Haider, A., van Hertem, D., *et al.*: 'Prospects and challenges of future HVDC SuperGrids with modular multilevel converters'. Proc. IEEE Power Electronics and Applications Conf., Birmingham, UK, 2011
13 Marquardt, R.: 'Modular multilevel converter: an universal concept for HVDC-networks and extended DC-bus-applications'. Proc. Int. Conf. on Power Electronics, Sapporo, Japan, 2010, pp. 502–507
14 Xu, J., Zhao, C., He, Z., *et al.*: 'Start-up control and DC fault ride-through strategies of a hybrid MMC-HVDC system suitable for overhead line transmission'. Second Int. Future Energy Electronics Conf. (IFEEC), Taipei, Taiwan, 2015
15 Jiang, B., Gong, Y., Cao, J., *et al.*: 'Fault current analysis of MMC based HVDC systems under DC pole-to-pole fault condition'. Int. Conf. on Renewable Power Generation (RPG), Beijing, China, 2015
16 Laterne, W., van Hertem, D.: 'Reduced modular multilevel converter model to evaluate fault transients in DC grids'. 12th IET Int. Conf. on Developments in Power System Protection (DPSP), Copenhagen, Denmark, 2014
17 Shi, X., Wang, Z., Liu, B., *et al.*: 'DC impedance modelling of a MMC-HVDC system for DC voltage ripple prediction under a single-line-to-ground fault'. IEEE Energy Conversion Congress and Exposition (ECCE), Pittsburgh, USA, 2014
18 Marten, A.-K., Vahrenholt, V., Fischer, W., *et al.*: 'Substation layout for multi-terminal HVDC systems and neutral conductor arrangements for reduced field emissions'. Proc. Int. Conf. on AC and DC Transmission, Birmingham, UK, 2015
19 Khatir, M., Zidi, S.A., Fellah, M.K., *et al.*: 'HVDC transmission line models for steady-state and transients analysis in SIMULINK environment'. Proc. IEEE Annual Conf. on Industrial Electronics, Paris, France, 2006, pp. 436–441
20 Sommer, R., Ammermann, D., Hennig, E.: 'More efficient algorithms for symbolic network analysis: Supernodes and reduced loop analysis, analog integrated circuits and signal processing', *Analog Integr. Circuits Signal Process.*, 1993, **3**, (1), pp. 73–83
21 CIGRÉ WG B4.58, Load flow control and direct voltage control in a meshed HVDC Grid, Draft version, 2015